JOURNAL OF AIRCRAFT
Vol. 38, No. 3, May–June 2001

# Micro-Air-Vehicles: Can They be Controlled Better?

Mohamed Gad-el-Hak*
*University of Notre Dame, Notre Dame, Indiana 46556*

**Micro-air-vehicles (MAV) are small, autonomous, aerial vehicles designed for reconnaissance and difficult to reach missions. Microelectromechanical systems (MEMS) are extremely small machines in which electronic and mechanical components are combined on a single silicon chip using photolithographic micromachining techniques. The question of whether MEMS can help improve the performance of futuristic MAV is pondered. The treatment focuses on the lifting and control surfaces of MAV, particularly the fixed-wing type. Two additional ideas are advanced to improve the performance of the lifting surfaces of MAV: effecting chaotic mixing to energize the laminar boundary layer and thus delay separation; and using genetic algorithms to optimize the shape of the airfoil section.**

## I. Introduction

INTENSIVE research has been conducted in the past few years to miniaturize uncrewed aerial vehicles (UAV). Existing remotely piloted UAVs such as the Predator, Hunter, or Pioneer have performed brilliantly in recent combat missions for the United States, but are too large as well as expensive for certain scientific sampling, monitoring, and surveillance tasks. The Predator, as an example, is 8.2 m long and has a wing span of 14.8 m and a cruise speed of about 35 m/s. Figure 1 is a photograph of the Predator, which was the highest flying, farthest ranging, longest loitering UAV used in Kosovo. Each unit costs $2 million and, having 7620-m ceiling, is considered a medium-altitude endurance UAV.[1] Although much smaller and slower than conventional aircraft, the Predator and its cousins are too large for certain search and rescue missions. Smaller, autonomous aircraft down to the size of birds and even insects are sought. These futuristic low-altitude drones are generally termed miniature- or micro-air-vehicles (MAV) and are intended for use by the military at the platoon level without unduly extensive training or by civilian search and rescue missions of, for example, earthquake victims. The accompanying lower Reynolds number presents numerous aerodynamic challenges to the designer of the airplane's lifting and control surfaces, thrust generator, and power plant.

In 1999, four prototype MAV were demonstrated in the United States: two fixed-wing, one rotorcraft, and one ornithopter type.[2] Lockheed Sanders' MicroSTAR and AeroVironment's Black Widow both have fixed wings of 0.15-m span. Their cruise speed is about 13 m/s, and their range is less than 5000 m. Figure 2 is a photograph of the Sanders MicroSTAR, which recently flew for 15 min under manual control and without an imaging payload. Lutronix Corporation tested a 0.15-m-diam rotorcraft. The 10-g Microbat ornithopter has a 0.15-m span, and its wings flap at a frequency of 20 Hz and is hoped to have eventually a hummingbirdlike vertical flight. At 300 g, the MAV helicopter is heavier than the prototypical 70-g fixed-wing MAV but carries up to 100-g payload including an infrared imager. In mass production, MAV are expected to cost around $3000 each. Though reusable, MAV drones do not present great loss if crashed or captured. Most important, there is no pilot life at risk.

To optimize the performance of those and similar drones, improvements may be made in their lifting and control surfaces, power plants, thrust generators, navigation systems, cameras, and data transmitting links. We focus on the lifting and control surfaces particularly for fixed-wing MAV. We ponder the question whether microelectromechanical systems (MEMS) can help achieving ever smaller and more efficient MAV. Ingenious flow control devices and control surfaces are sought at the exceedingly low Reynolds numbers associated with MAV. This is not a trivial task because flow separation and low lift-to-drag ratio are notoriously associated with low chord Reynolds number. Moreover, any control device employed must meet strict weight and space limitations as evidenced from the specifications quoted earlier for the four prototypical MAVs. One possible scenario is to effect beneficial flow control, particularly separation prevention or delay, using microsensors and microactuators in closed control loops instead of traditional passive or open-loop control strategies. Microactuators can also be used instead of bulky control surfaces such as the traditional mechanical flaps acting as ailerons, elevators, and rudders to control the aircraft's roll, pitch, and yaw, respectively.

In the following section, we outline some aerodynamic considerations associated with low Reynolds number MAV. Section III briefly discusses recent developments in MEMS and the possible use of such systems to delay separation on MAV. Two novel ideas on chaotic mixing and shape optimization using genetic algorithms are introduced in Secs. IV and V, respectively. Finally, concluding remarks are given in Sec. VI.

## II. Aerodynamic Considerations

Insects, birds, and bats have perfected the art of flight through millions of years of evolution. Human's dream of flying dates back to the early Greek myth of Daedalus and his son Icarus, but the first successful heavier-than-airflight took place less than a century ago. Today, the Reynolds numbers for natural and fabricated fliers span the amazing range from $10^2$ to $10^9$; insects are at the low end of this spectrum, and huge airships occupy the high end.[3]

Consider a fixed-wing airplane. The typical chord Reynolds number for a commercial aircraft is $Re_c \equiv U_\infty c/\nu = \mathcal{O}(10^7)$, where $U_\infty$ is the cruising speed, $c$ is the wing chord, and $\nu$ is the air kinematic viscosity. For the remotely piloted Predator, $Re_c = \mathcal{O}(10^6)$. For insects, $Re_c < 10^4$. MAV would probably have chord Reynolds number in the range of $10^4$–$10^5$. The low Reynolds number associated with those autonomous drones presents numerous challenges because of the concomitant susceptibility of their lifting surfaces to flow separation and lower efficiency.

The function of the airfoil section on those fliers is to produce lift. Inevitably, viscous effects, compressibility effects, and the finite span of the lifting surface all ensure that drag is also produced. A thrust must be generated by some sort of a power plant to overcome this streamwise resistance to the motion. The lift-to-drag ratio is a measure of the effectiveness of the airfoil. In general, this ratio is very low at low Reynolds numbers and improves with increases in this parameter. As shown in Fig. 3, reproduced from McMasters and Henderson,[4] the maximum lift-to-drag ratio $[C_L/C_D]$ improves dramatically in the range of chord Reynolds numbers of $Re_c = 10^4$–$10^6$.

Received 1 May 2000; revision received 22 August 2000; accepted for publication 8 September 2000. 

*Professor, Department of Aerospace and Mechanical Engineering. Associate Fellow AIAA.

**Fig. 1 Medium-altitude endurance UAV Predator with 14.8-m wing span.**

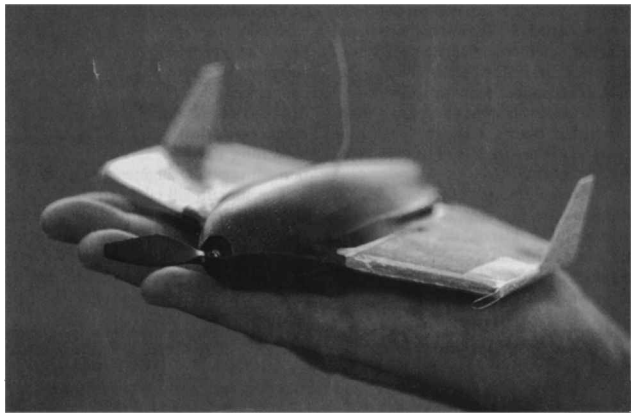

**Fig. 2 Sanders MicroSTAR with 0.15-m wing span resting on a human hand.**

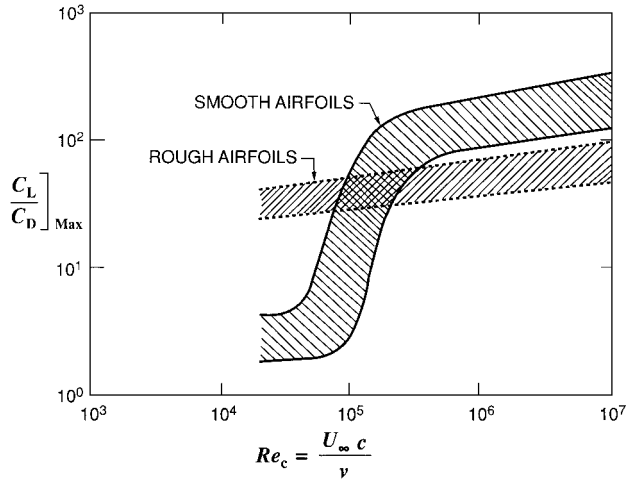


**Fig. 3 Airfoil performance as function of chord Reynolds number (from McMasters and Henderson[4]).**

Below $10^4$, typical of insects and small model airplanes, the boundary layer around the lifting surface is laminar. Stalling in this case is caused by an abrupt separation of the laminar flow near the leading edge as the angle of attack is increased to modest values. (The arguments and the cited value are for steady-state flows. Insects and other very low Reynolds number fliers exploit unsteady effects to achieve remarkable performances. At the extremely low Reynolds number $Re$ typical of small insects, viscous forces begin to dominate over inertial ones. Clearly, such insects exploit unconventional sources of lift.[5]) The maximum lift is limited, and the drag increases significantly when the lifting surface stalls.

For $Re_c > 10^6$, typical of large aircraft, boundary layer transition to turbulence usually takes place ahead of the theoretical laminar separation point. A turbulent boundary layer can negotiate quite severe adverse pressure gradients without separation, and this kind of lifting surface often experiences a trailing-edge stall at relatively high angles of attack. The stall is preceded by a movement of the separation point forward from the trailing edge with increasing incidence.[6]

In the range of Reynolds numbers of $10^4$–$10^6$, termed low Reynolds number[7] for the purpose of this paper, many complicated phenomena take place within the boundary layer. Separation, transition, and reattachment can all occur within a short distance and can dramatically affect the performance of the lifting surface. The laminar separation bubble that commonly forms in this range of Reynolds numbers plays an important role in determining the boundary-layer behavior and the stalling characteristics of the airfoil.[8] As indicated in Fig. 3, the maximum lift-to-drag ratio for a smooth airfoil increases by two orders of magnitude in this Reynolds number regime. Remotely piloted aircraft, MAV, and turbine blades are examples of lifting surfaces having this range of Reynolds numbers.

The skilled designer has available a variety of passive and active techniques to effect a beneficial change in the complex flowfield that characterizes this intermediate range of Reynolds numbers. Roughness and shaping are among the simplest passive methods to ensure flow attachment beyond a critical angle of attack and, thus, an improved performance. Wall transpiration and heat transfer are examples of active control methods to improve the lift-to-drag ratio. Although these broad flow control strategies are similar to those employed at much higher Reynolds number $Re$, the emphasis here is on the low Reynolds number regime dominated by the formation of laminar separation bubbles.

The present paper discusses the aerodynamics of low Reynolds number lifting surfaces, particularly the formation and control of separation bubbles. Flow control goals in those cases are strongly interrelated leading to certain difficulties in choosing the best control strategy for a particular end result. These potential conflicts are detailed in a second paper by the author in this volume.[9]

### A. Low Reynolds Number Airfoils

What is considered low Reynolds number is of course in the eye of the beholder. For a chemical engineer, $Re \ll 1$ might be considered low Reynolds number. For a boundary-layer analyst, $Re < 1000$ might be called low Reynolds number. For the designer of a MAV, $Re < 10^5$ might be considered low Reynolds number.

In the range of chord Reynolds numbers of $Re_c = 10^4$–$10^6$, a substantial improvement in the lift-to-drag ratio of an airfoil takes place. According to Carmichael,[3] this is the Reynolds number regime where we find humans and nature together in flight: large soaring birds, large radio-controlled model aircraft, foot-launched ultralight, human-carrying hang gliders, human-powered aircraft, and the more recently developed remotely piloted vehicles, as well as the autonomous MAV used for military and scientific sampling, monitoring, and surveillance. Four review articles on low-Reynolds-number aerodynamics by Tani,[8] Lissaman,[7] Mueller,[10] and Gad-el-Hak[11] are particularly recommended. There is also a wealth of information available in the proceedings of the various conferences dedicated to the subject matter (see Refs. 12–14 and the International Conference on Aerodynamics at Low Reynolds Numbers $10^4 < Re < 10^6$, Royal Aeronautical Society, London, 15–18 October 1986, and the Eighth International Conference on Remotely Piloted Vehicles, Bristol, England, United Kingdom, 2–4 April 1990).

In this range of Reynolds numbers, very complex flow phenomena take place within a short distance on the upper surface of an airfoil at incidence. Unless artificially tripped, the boundary layer remains laminar at the onset of pressure recovery, and the airfoil's performance is then entirely dictated by the laminar flow's poor resistance to separation. The separated flow forms a free-shear layer, which is highly unstable, and transition to turbulence is readily realized. Subsequent reattachment of the separated region may take place because of the increased entrainment associated with the turbulent flow. Provided that the high-speed fluid entrained into the wall region supplies sufficient energy to maintain the circulating motion against dissipation, a separation bubble forms.

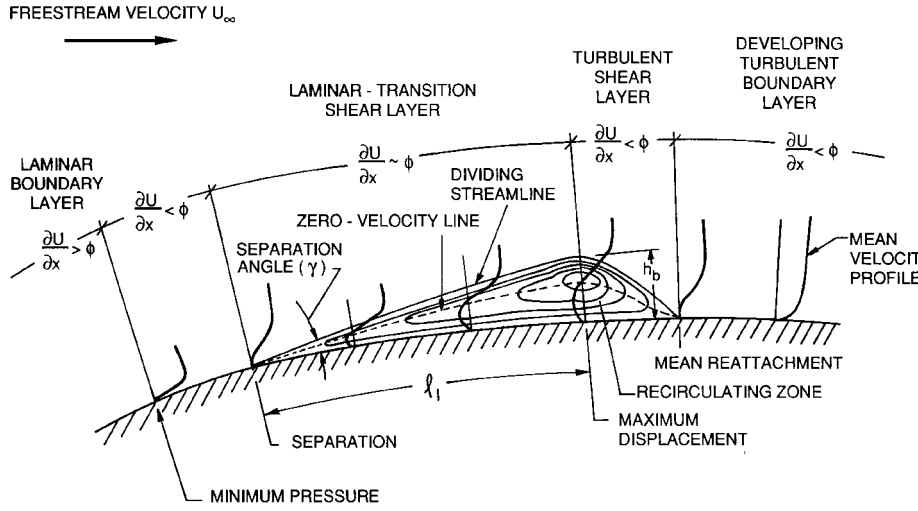


**Fig. 4 Laminar separation bubble.**

In other words, for the formation of a laminar separation bubble, the precise conditions for the occurrence of separation, transition, and reattachment depend on the Reynolds number, the pressure distribution, the surface curvature, the surface roughness, and the freestream turbulence, as well as other environmental factors. If the Reynolds number is sufficiently high, transition takes place near the minimum pressure point ahead of the location at which separation would have occurred if the boundary layer had remained laminar. For moderate Reynolds numbers, separation takes place before transition. The laminar boundary layer can only support a very small adverse pressure gradient without separation. It is well known that if the ambient incompressible fluid decelerates in the streamwise direction faster than $U_0 \sim x^{-0.09}$, the flow separates. The separated flow will not reattach to the surface and no bubble will be formed if the Reynolds number is sufficiently low. However, for the intermediate Reynolds number range (typically $10^4$–$10^6$), the separated flow proceeds along the direction of the tangent to the surface at the separation point,[15] and transition to turbulence takes place in the free-shear layer due to its increased transition susceptibility. Subsequent turbulent entrainment of high-speed fluid causes the flow to return to the surface, thus forming what is known as a laminar separation bubble, as shown in Fig. 4. Downstream of the point of reattachment, the newly formed turbulent boundary layer is capable of negotiating quite severe adverse pressure gradients without separation. The ability of a turbulent boundary layer to resist separation improves as the Reynolds number increases.[7]

### B. Conditions for Bubble Formation

It is clear from the preceding arguments that bubble formation is confined to a certain range of Reynolds numbers and that this range changes from one airfoil to another as well as from one environment to another. A rough rule according to Carmichael[3] is that the Reynolds number based on freestream velocity and the distance from separation to reattachment is approximately $5 \times 10^4$. In general, then, an airfoil with chord Reynolds number less than $5 \times 10^4$ will experience laminar separation with no subsequent reattachment. For chord Reynolds numbers slightly higher than $5 \times 10^4$, a long bubble is expected. Shorter bubbles are formed at higher Reynolds numbers. Tani[8] asserts that a Reynolds number typical of local conditions in the boundary layer is more appropriate to characterize a separation bubble than the chord Reynolds number. Typically, the Reynolds number, based on the boundary-layer's displacement thickness and the velocity just outside the rotational flow region at the point of separation, is more than 500 for a short bubble and less than 500 for a long one. [Note that the displacement thickness $\delta^*$ for a laminar boundary layer near the leading edge of an airfoil is extremely small and cannot be accurately measured. Instead the momentum thickness $\delta_\theta$ is computed from the pressure distribution using Thwaites's formula,[16] and the ratio $(\delta^*/\delta_\theta)$ at the separation point is assumed to be 3.7. Also, the bubble gets shorter at higher Reynolds number $Re_{\delta^*}$; at $Re_{\delta^*} \approx 6000$, bubble formation is precluded (bubble's streamwise extent approaches zero) by transition to turbulence in the boundary layer.] The corresponding bubble's streamwise extent, normalized with the displacement thickness at the point of separation, is $10^2$ and $10^4$, respectively.[8]

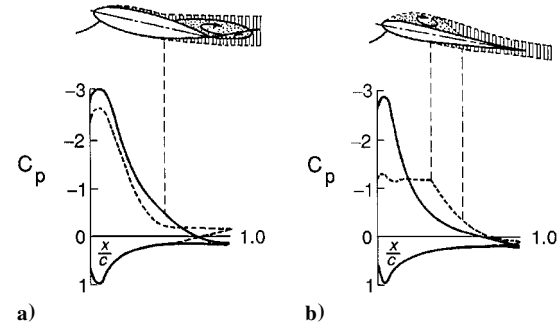


**Fig. 5 Qualitative pressure distributions for two airfoils at incidence, (——) potential flow solution and (– – –) experiment: a) short bubble on upper surface and subsequent rear separation of turbulent boundary layer and b) long bubble.**

The short separation bubble generally has a length of the order of a few percent of the chord. It merely represents a transition-forcing (tripping) mechanism to allow reattachment of an otherwise separated shear layer. Such a bubble does not greatly affect the peak suction as determined from the potential flow solution around the airfoil. Except for the appearance of a minute bump in the lift curve ($C_L$ vs $\alpha$ curve, where $C_L$ is the lift coefficient and $\alpha$ is the angle of attack), the presence of a short bubble has no significant effect on the pressure distribution around the lifting surface, as shown in Fig. 5a. On the other hand, a long bubble may be as much as $0.2c$–$0.3c$, where $c$ is the airfoil chord, and significantly changes the pressure distribution by effectively altering the shape over which the outer potential flow is developed. In this case, the sharp suction peak near the leading edge is generally not realized, and a suction plateau of a reduced level extends over the region occupied by the bubble (Fig. 5b). A long bubble tends to increase in length as incidence is increased, leading to a corresponding decrease in the slope of the lift curve as well as an increase in the pressure drag.

Interestingly, recent experiments[17] indicate that thin, low-aspect-ratio wings, such as those contemplated for MAV, may not suffer from serious stall or separation bubble problems even at exceedingly low Reynolds numbers. The lift for thin wings having aspect ratios less than 2 is dominated by the tip vortices. Such wings are not that different aerodynamically from delta wings: difficult to stall but quite susceptible to rolling instabilities (wobbling). Thus, whereas the control of separation bubble described here may not be relevant

to low-aspect-ratio wings, stabilizing the rolling motions of those wings may be crucial. On the other hand, design considerations may dictate the use of wings having aspect ratios larger than 2, and the following control strategies may then prove useful.

### C. Bubble's Breakdown

In general, the lift-to-drag ratio is higher for an airfoil having a shorter bubble. Depending on many factors, a short bubble forming at low incidence may move forward and contract in streamwise extent as the angle of attack is increased.[8] Within the bubble, a small region of constant pressure exists followed by pressure recovery. At higher incidence, the bubble bursts and no longer reattaches, thus ensuing a leading-edge stall.[18] This process is often irreversible, which means that reducing the angle of attack will not immediately unburst the bubble. Strong lift hysteresis effects are, therefore, observed as the attack angle or the Reynolds number is recycled.[19–22] Similar hysteresis effects are also seen in drag.

For thin airfoils of small nose radius, pressure recovery commences very near the leading edge, and the adverse pressure gradients are severe at high angles of attack. Separation bubble may occur on these airfoils even at chord Reynolds numbers exceeding $10^6$. At large incidence, the short bubble breaks down into a long one. With increasing angles of attack, the reattachment point moves progressively backward until it reaches the trailing edge, at which stage its maximum thickness is typically 3% of the chord. A further increase in incidence leads to completely detached flow and the so-called thin-airfoil stall. A comprehensive review of the different kinds of stall on thin airfoils is given by Crabtree.[23]

Aerodynamics data for both thin and thick airfoils in the low Reynolds number regime are accessible in several recent papers and conference proceedings (for example, see Refs. 12–14 and 24–30). Available experimental data on bubble's formation and bursting indicates that transition to turbulence in the separated shear-layer and subsequent reattachment will occur if the Reynolds number based on displacement thickness at the point of laminar separation exceeds a critical value that is not necessarily universal (Tani–Owen–Klanfer criterion[8]). A lower limit for this Reynolds number seems to be $Re_{\delta^*} \approx 350$. Bursting occurs if the pressure recovered in the reattachment process in terms of the dynamic pressure at separation (pressure recovery coefficient) exceeds a certain critical value (Crabtree criterion). Again, this critical value changes from one airfoil to another, but an upper limit of 0.35 appears to be valid for many shapes. Crabtree[31] assumes that bubble's breakdown occurs because there exists a maximum possible value of pressure that can be recovered in the turbulent entrainment process that causes the flow reattachment. This implies the existence of a maximum possible value of the shear stress set up in the turbulent entrainment region so as to counteract the pressure gradient. At breakdown, caused by either an increase in incidence or a decrease in Reynolds number, the Tani–Owen–Klanfer criterion is satisfied, but the Crabtree criterion is about to be violated.

The question of primary concern to us in this paper is how to control the flow around a low Reynolds number airfoil to achieve improved performance. The interrelation between the different control goals is particularly salient when a separation bubble exists. According to Tani,[8] all three kinds of stall, trailing-edge stall, leading-edge stall, and thin-airfoil stall, may occur for a given airfoil at different Reynolds numbers or for different airfoils at a given Reynolds number. A particular lifting surface produces higher lift at higher incidence, limited by the angle at which the airfoil stalls. At that point, drag increases dramatically, and the lifting surface performance deteriorates rapidly. Flow control is aimed at improving this performance. Among the practical considerations that must be considered for both active and passive control devices are their cost of construction and operation, complexity, and potential tradeoffs or penalties associated with their use. It is this latter point in particular that presents an additional degree of complexity for controlling low Reynolds number lifting surfaces. Achieving a beneficial effect for one control goal may very well adversely affect another goal, and design compromises must often be made. Those issues are discussed in more detail in Ref. 9.

### D. Separation Control

Fluid particles in a boundary layer are slowed down by wall friction. If the external potential flow is sufficiently retarded, for example, due to the presence of an adverse pressure gradient, the momentum of those particles will be consumed by both the wall shear and the pressure gradient. At some point (or line), the viscous layer departs or breaks away from the bounding surface. The surface streamline nearest to the wall leaves the body at this point, and the boundary layer is said to separate. At separation, the rotational flow region next to the wall abruptly thickens, the normal velocity component increases, and the boundary-layer approximations are no longer valid. Because of the large energy losses associated with boundary-layer separation, the performance of a lifting surface is often controlled by the separation location. If separation is postponed, the pressure drag is decreased and the circulation and, hence the lift at high angles of attack, is enhanced.

Separation control methods include the modulation of pressure gradient via shaping, wall suction, surface cooling in gases, and surface heating in liquids. The first of these strategies is the simplest and is most suited for low Reynolds number situations. Streamlining can greatly reduce the steepness of the pressure rise. In contrast to turbulent flows, laminar boundary layers can only support very small adverse pressure gradients without separation. Transition on the upper surface of a lifting surface typically occurs at the first onset of adverse pressure gradient if the Reynolds number exceeds $10^6$. The separation-resistant turbulent boundary layer that evolves in the pressure recovery region results in higher maximum lift at relatively large angle of stall. Depending on the severity of the initial adverse gradient, and hence on the airfoil shape, laminar separation may take place before transition. Regardless of whether or not the flow subsequently reattaches, the laminar separation leads to higher form drag and lower maximum lift. Delicate contouring of the airfoil near the minimum pressure point to lessen the severity of the adverse pressure gradient may be used to accomplish separation-free transition.

As an example of the effects of the lifting surface's shape on its performance, consider the lift curves for the three airfoil sections: NACA $63_3$-018, NACA 63-009, and NACA 64A006. These airfoils have maximum thicknesses of $0.18c$, $0.09c$, and $0.06c$, respectively, where $c$ is the chord. The respective leading-edge radii are $0.021c$, $0.006c$, and $0.003c$. Figure 6, adapted from the measurements by McCullough and Gault,[6] shows $C_L$ vs $\alpha$ curves for the three sections at chord Reynolds number of $5.8 \times 10^6$. For the thick section, NACA $63_3$-018, transition takes place near the minimum pressure point.[32] Stalling in this case is of the trailing-edge type and is preceded by a gradual movement of the separation point of the turbulent boundary layer forward from the trailing edge as $\alpha$ increases. A laminar separation bubble is formed on the other two sections at small incidence. However, the NACA 63-009 section experiences a sudden leading-edge stall when the bubble bursts with no subsequent reattachment, whereas the NACA 64A006 section experiences a more gradual

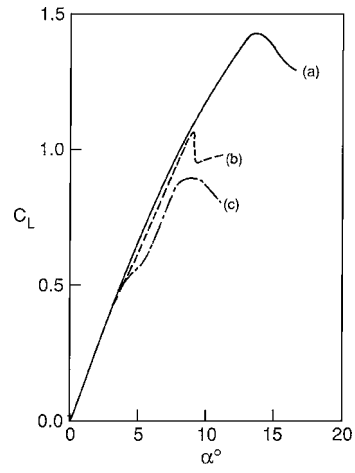


**Fig. 6 Lift curves for three airfoils at $Re_c = 5.8 \times 10^6$: a) NACA $63_3$-018, b) NACA 63-009, and c) NACA 64A006 (adapted from McCullough and Gault[6]).**

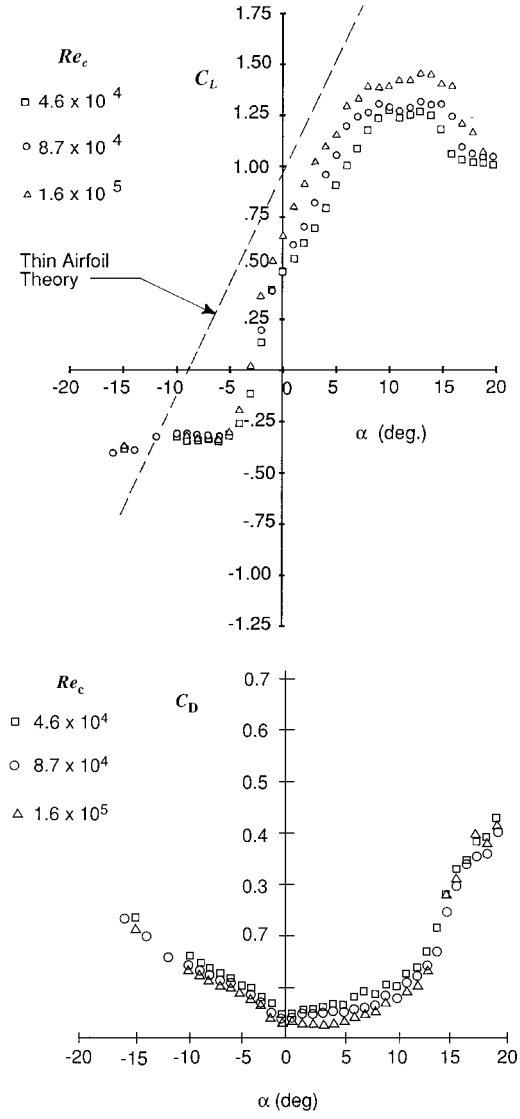


**Fig. 7 Reynolds number effects on lift (top curves) and drag (bottom curves) of the Eppler 61 airfoil (adapted from Mueller and Burns[25]).**

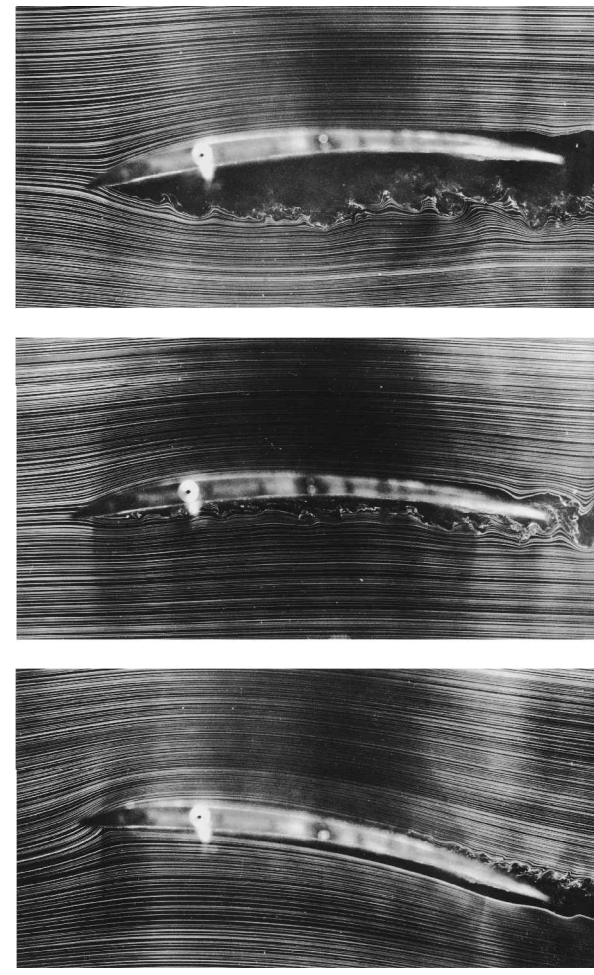

**Fig. 8 Smoke-wire flow visualization of the low Reynolds number Eppler 61 airfoil, $Re_c = 8.7 \times 10^4$: a) $\alpha = -3$ deg, b) $\alpha = 0$ deg, and c) $\alpha = 8$ deg (from Mueller and Burns[25]).**

thin-airfoil stall.[23,33] In the latter case, the short bubble breaks down into a longer bubble at an angle of attack of 5 deg causing a slight discontinuity in the lift curve. Subsequent increase in $\alpha$ leads to a movement of the reattachment point toward the trailing edge. The maximum lift in this case is about 40% lower than that for the thick airfoil. The stall angle is also lower.

A second example is provided for an airfoil specifically designed for the low Reynolds number regime. The carefully contoured Eppler 61 has a maximum thickness of 0.056$c$ and is highly cambered. Mueller and Burns[25] reported lift, drag, and smoke visualization data for this airfoil section in the range of Reynolds numbers of $3 \times 10^4$–$2 \times 10^5$. A sample of their lift and drag curves at three different speeds is shown in Fig. 7. At a negative angle of attack of about $\alpha = -3$ deg, the flow around the cambered airfoil separates at the leading edge on the lower surface, without further reattachment. Zero lift is measured at this angle and is correlated with the appearance of smooth smokelines above and below the airfoil to form an uncambered, symmetrical shape, as shown in the top photograph in Fig. 8. In Fig. 8, the chord Reynolds number is $Re_c = 8.7 \times 10^4$, and three angles of attack are shown: $\alpha = -3$, $\alpha = 0$, and $\alpha = 8$ deg. The results explain the deviation of the zero-lift angle as well as the shape of the lift curve from those predicted by thin-airfoil theory. Strong Reynolds number effects are evident in both the lift and drag curves. At increasing angles of attack, the performance of the Eppler 61 airfoil is similar to that of the other thin airfoil shown in Fig. 6c, although the maximum lift coefficient is higher in the former case.

## III. Microfabrication

Manufacturing processes that can create extremely small machines have been developed in recent years.[34–46] In this emerging microfabrication technology, under intensive development only since 1990, electronic and mechanical components are combined on a single silicon chip using photolithographic micromachining techniques. Motors, electrostatic actuators, pneumatic actuators, valves, gears, and tweezers of typical size $\mathcal{O}(10\ \mu\text{m})$ have been fabricated. These have been used as sensors for pressure, temperature, velocity, mass flow, or sound, and as actuators for linear and angular motions. Current usage for MEMS includes accelerometers for airbags and guidance systems, pressure sensors for engine air intake and blood analysis, rate gyroscopes for antilock brakes, microrelays and microswitches for semiconductor automatic test equipment, and microgrippers for surgical procedures.[37,41,47–51] There is considerable work under way to include other applications, one example being the microsteam engine described by Lipkin.[52] A second example is the $3 \times 1.5$ cm digital light processor, which contains $0.5$–$2 \times 10^6$ individually addressable micromirrors, each measuring 16 $\mu$m on a side. Texas Instruments, Inc., is currently producing such device with a resolution of $2000 \times 1000$ pixel, for high-definition televisions and other display equipments. The company maintains that when mass produced, such device costs on the order of $100, that is, less than $0.0001 per actuator.

The new *Journal of Microelectromechanical Systems* and *Journal of Micromechanics and Microengineering* are dedicated to this technology, and the older *Sensors and Actuators* is increasingly

allotting more of its pages to MEMS. Entire sessions in scientific meetings have been increasingly assigned to MEMS applications in fluid mechanics (see, for example, the presentations by McMichael, Tai, Mehregany, Mastrangelo, and Yun, all made at the AIAA Third Shear Flow Control Conference, Orlando, Florida, 6–9 July 1993, and Refs. 53 and 54). Recent reviews of the use, or potential use, of MEMS in flow control include those by Gad-el-Hak,[55–57] Lumley,[58] McMichael,[59] Mehregany et al.,[60] and Ho and Tai.[42,43]

MEMS would be ideal for the reactive flow control concept advocated in the present paper (see Gad-el-Hak[9] for a concise explanation of the distinction between predetermined and reactive control and the different control loops involved in each). Methods of flow control targeted toward specific separation events involve nonintrusive detection and subsequent modulation of events that occur randomly in space and time. To achieve proper targeted control of these quasi-periodic vortical events, temporal phasing as well as spatial selectivity are required. Practical implementation of such an idea necessitates the use of a number of intelligent, communicative wall sensors and actuators arranged in a checkerboard pattern.

The sensors would be expected to measure the amplitude, location, and phase or frequency of the signals impressed on the wall by incipient separation events. Instantaneous wall-pressure or wall-shear stress can be sensed, for example. The normal or in-plane motion of a minute membrane is proportional to the respective point force of primary interest. For measuring wall pressure, microphonelike devices respond to the motion of a vibrating surface membrane or an internal elastomer. Several types are available including variable-capacitance (condenser or electret), ultrasonic, optical (e.g., optical-fiber and diode-laser), and piezoelectric devices (for example, see Löfdahl et al.[61,62] and Löfdahl and Gad-el-Hak[63,64]). A potentially useful technique for our purposes has been tried at Massachusetts Institute of Technology.[65–68] An array of extremely small (0.2 mm in diameter) laser-powered microphones (termed picophones) was machined in silicon using integrated circuit fabrication techniques and was used for field measurement of the instantaneous surface pressure in a turbulent boundary layer. The wall-shear stress, though smaller and, therefore, more difficult to measure than pressure, provides a more reliable signature of the near-wall events.

Actuators are expected to produce a desired change in the targeted separation events. The local acceleration action needed to prevent an incipient separation can be in the form of adaptive wall, transpiration, wall heat transfer, or electromagnetic body force. Traveling surface waves can be used to modify a locally convecting pressure gradient such that the wall motion follows that of the targeted event causing the pressure change. Surface motion in the form of a Gaussian hill with a dimensionless (viscous) height of $y^+ = \mathcal{O}(10)$ should be sufficient to suppress typical incipient separation. Such time-dependent alteration in wall geometry can be generated by driving a flexible skin using an array of piezoelectric devices (dilate or contract depending on the polarity of current passing through them), electromagnetic actuators, magnetoelastic ribbons (made of nonlinear materials that change their stiffness in the presence of varying magnetic fields), or Terfenol-d rods (a novel metal composite, which changes its length when subjected to a magnetic field developed at Grumman Corporation). Note should also be made of other exotic materials that can be used for actuation. For example, electrorheological fluids[69] instantly solidify when exposed to an electric field and may thus be useful for the present application. Recently constructed microactuators specifically designed for flow control include those by Wiltse and Glezer,[70] James et al.,[71] Jacobson and Reynolds,[72] Vargo and Muntz,[73] and Keefe.[74]

Suction/injection at many discrete points can be achieved by simply connecting a number of minute streamwise slots, arranged in a checkerboard pattern, to a low-pressure/high-pressure reservoir located underneath the working surface. The transpiration through each individual slot is turned on and off using a corresponding number of independently controlled microvalves. Alternatively, positive-displacement or rotary micropumps (for example, see Sen et al.[75] and Sharatchandra et al.[76,77]) can be used for blowing or sucking fluid through small holes/slits.

Finally, if separation is to be delayed by lowering the near-wall viscosity, direct electric-resistance heating can be used in liquid flows and thermoelectric devices based on the Peltier effect can be used for cooling in the case of gaseous boundary layers. The absolute viscosity of water at 20°C decreases by approximately 2% for each 1°C rise in temperature, whereas for room-temperature air, $\mu$ decreases by approximately 0.2% for each 1°C drop in temperature. The streamwise momentum equation written at the wall can be used to show that a suction coefficient of 0.0006 has approximately the same effect on the wall curvature of the instantaneous velocity profile as a surface heating of 2°C in water or a surface cooling of 40°C in air.[78,79]

Sensors and actuators of the types discussed in this section can be combined on individual electronic chips using microfabrication technology. The chips can be interconnected in a communication network that is controlled by a massively parallel computer or a self-learning neural network, perhaps each sensor/actuator unit communicating only with its immediate neighbors. In other words, it may not be necessary for one sensor/actuator to exchange signals with another far away unit. Factors to be considered in an eventual field application of chips produced using microfabrication processes include sensitivity of sensors, sufficiency and frequency response of actuators' action, fabrication of large arrays at affordable prices, survivability in the hostile field environment, and energy required to power the sensors/actuators. As argued by Gad-el-Hak,[55,57] sensor/actuator chips currently produced are small enough for typical field application, and they can be programmed to provide a sufficiently large/fast action in response to a certain sensor output (also see Jacobson and Reynolds[72]). Present prototypes are, however, still quite expensive as well as delicate. However so was the transistor when first introduced. It is hoped that the unit price of future sensor/actuator elements would follow the same dramatic trends witnessed in case of the simple transistor and even the much more complex integrated circuit. The price anticipated by Texas Instruments for an array of $1 \times 10^6$ mirrors hints that the technology is well in its way to mass produce phenomenally inexpensive microsensors and microactuators. Additionally, current automotive applications are a rigorous proving ground for MEMS: Under-the-hood sensors can already withstand harsh conditions such as intense heat, shock, continual vibration, corrosive gases, and electromagnetic fields.

## IV. Chaotic Mixing

For the purpose of energizing a laminar boundary layer to prevent separation, stirring by chaotic advection may be an attractive alternative for situations where turbulence is either not possible or not desired. We outline in this section the concept of chaotic mixing. Minute geometrical modifications on a lifting surface may be used to effect such mixing and thus delay separation. The idea here is to effect chaotic particle paths even for well-behaved velocity fields. A group of adjacent particles in chaotic motion will tend to deviate exponentially from one another, and this leads to substantial mixing with the surrounding fluid in a much shorter time than would be expected for regular motion. The resulting transport can be more effective than that in ordinary laminar flows even those with superimposed secondary motions. The concept of chaotic advection has been demonstrated theoretically, experimentally, and numerically for mass and energy transport. Chaotic advection, or Lagrangian chaos, is possible for time-dependent, two-dimensional (or three-dimensional) flowfields as well as for steady, three-dimensional flows.

Consider the diffusion equation for a passive scalar field $\theta(\boldsymbol{x}, t)$ having a constant diffusivity $\mathcal{D}$. In the Eulerian description, the partial differential equation that governs the diffusion process is linear because the velocity field is obtained independently from the continuity and momentum equations. The diffusion equation with no source terms reads

$$\frac{\partial \theta}{\partial t} + \boldsymbol{u} \cdot \nabla \theta = \mathcal{D} \nabla^2 \theta \tag{1}$$

where the advecting velocity field $\boldsymbol{u}(\boldsymbol{x}, t)$ is a prescribed function of the spatial coordinates $\boldsymbol{x}$ and time $t$. In a turbulent flow, $\boldsymbol{u}$ is a random

vector field, and therefore, $\theta$ is also expected to be random. However, the surprising result, considering the linearity of the governing equation, is that the scalar field $\theta$ can exhibit chaotic behavior even for simple laminar flows. This was demonstrated rather elegantly by Aref,[80] who coined the expression chaotic advection.

When the problem of a passively transported tracer is analyzed from a Lagrangian viewpoint, the governing equations may be nonlinear and nonintegrable. The resulting Lagrangian chaos is a spatial not a temporal one. Therefore, Eq. (1) is not the proper dynamical system to represent the problem, and its linearity or lack thereof is irrelevant to the chaotic behavior of $\theta$. The velocity at a point may be constant or periodic, whereas the passively transported scalar may be aperiodic, that is, chaotic, in space. Consider the trajectories of individual advected particles

$$\frac{\mathrm{d}X}{\mathrm{d}t} = u(x, y, z, t) \tag{2}$$

$$\frac{\mathrm{d}Y}{\mathrm{d}t} = v(x, y, z, t) \tag{3}$$

$$\frac{\mathrm{d}Z}{\mathrm{d}t} = w(x, y, z, t) \tag{4}$$

The initial conditions are $\boldsymbol{X}|_{t=0} = \boldsymbol{X}_0$. These equations describe a finite-dimensional dynamical system and are the Lagrangian equivalent of Eq. (1) for the case of zero diffusivity. Chaotic particle paths lead to chaotic spatial distribution of the transported tracer.

The preceding equations are deterministic, which means the forcing terms on the right-hand side are not random, for nonturbulent velocity fields. For steady, two-dimensional flow, the streamlines and particle paths coincide (as they also do in steady, three-dimensional flows). The equations for particle paths can in this case be written in terms of the stream function, $\psi(x, y)$,

$$\dot{X} = \frac{\partial \psi}{\partial y}, \qquad \dot{Y} = -\frac{\partial \psi}{\partial x} \tag{5}$$

In the language of dynamical systems theory, the preceding equations are just Hamilton's canonical equations for one degree of freedom and, hence, are integrable when autonomous. Therefore, regular velocity field leads to regular passive scalar distribution. On the other hand, if the two-dimensional flowfield is time dependent, however innocuous, the nonautonomous Hamiltonian dynamic system can be nonintegrable producing stochastic particle paths. Note that for plane flow, the phase-space flow of a Hamiltonian dynamical system corresponds to the configuration-space motion of advected particles. For three-dimensional flows, both steady and unsteady laminar velocity fields can result in chaotic particle paths and, therefore, highly complex distribution of the passively transported tracer. In the steady case, a regular three-dimensional velocity field can produce chaotic particle paths and identically irregular streamlines, an amazing counterintuitive effect. These results provide a remarkable contrast between the Eulerian and Lagrangian representation of the same flow: Regular Eulerian flowfields can, under the right circumstances, lead to highly irregular advection patterns.

Unlike the fractal dimension test, which can only be used in dissipative dynamical systems, the Lyapunov exponent provides a quantitative criterion for the presence of chaos in both conservative (Hamiltonian) and dissipative deterministic systems. A positive exponent implies chaotic dynamics and measures the sensitivity of the system to changes in its initial conditions. If the initial distance between two trajectories in phase space is $d_0$, at a small but later time the distance is on the average

$$d(t) = d_0\, e^{\lambda t} \tag{6}$$

where $\lambda$ is the Lyapunov exponent. In the mixing problem, the Lyapunov exponent can be used to measure the rate at which an infinitesimal fluid volume is stretched. Each dimension of the flow has an associated exponent, and for a conservative, incompressible dynamical system, the sum of all exponents must be zero. For a nonchaotic system, stretching occurs at a linear rate, and thus, all Lyapunov exponents must be zero. For a system that exhibits chaotic particle paths, the largest Lyapunov exponent is positive, denoting exponential separation of neighboring particles. The exponent must, therefore, be negative in at least one other dimension, implying a diminution of length scale in that direction.

When the two-dimensional or three-dimensional laminar flowfield is chosen cleverly, the dynamical system (2–4) becomes nonintegrable with resulting stochastic response in the Lagrangian advection characteristics of a passively transported tracer. In this case, a group of adjacent particles will tend to deviate exponentially from one another, and this leads to substantial mixing with the surrounding fluid in a much shorter time than would be expected for regular motion. The resulting tremendous stretching of finite fluid regions paves the way for an enhanced activity by diffusion due to greater surface area and gradient available for the molecular processes. Despite the exponential divergence of neighboring states (in phase space), the stretching (that is divergence of neighboring trajectories) and folding (that is confinement to bounded space) mechanism is necessary to keep chaotic trajectories within a finite volume of phase space. The stretching and folding operation corresponds to what is called in dynamical systems theory a horseshoe map. Chaotic mixing can result from the breakup of homoclinic or hetroclinic loops into tangles. Those entanglements result from repeated intersections of the stable and unstable manifolds giving rise to chaotic behavior. This causes a set of particles to be spatially well mixed as it is advected by even an innocuous flowfield.

The utility of chaotic advection has been demonstrated for mass as well as energy transport. Chaotic mixing can be effected even at extremely low Reynolds or Péclet numbers where turbulence is not a viable option, which makes the technique particularly useful for a range of applications in chemical engineering, low-speed flows, heat transfer, and materials processing. Because Lagrangian chaos can be achieved even at extremely low speeds, the enhanced scalar transport is not necessarily associated with enhanced momentum transport. This is a tremendous practical advantage. In contrast, scalar transport enhancement by turbulence is often at the expense of significant pressure drop and/or skin-friction increase and, therefore, power expenditure.

We recall just a few of the recent deluge of demonstrations. The original analytical work in the field of chaotic advection is, as indicated earlier, due to Aref,[80] who also sites several earlier contributions by other researchers. Aref idealized an incompressible, inviscid fluid being stirred in a tank using point vortex agitator(s). Together with their images in the bounding contour, the agitators provide the source of unsteady potential flow. The motion is assumed wholly two dimensional. Aref demonstrated by way of a numerical integration of the time-dependent version of Eq. (5) that chaotic particle motions are possible for certain unsteady movements of the stirring vortex. Two protocols were used to generate the successful unsteadiness: either a stirrer that jumps back and forth between two fixed positions or two stirrers at fixed positions that are run alternately for a given time interval. In either case, efficient stirring was achieved when chaotic particle paths were generated using the successful protocol.

Ottino[81–83] details the body of analytical and experimental work conducted by his research group. Chaotic mixing of both miscible and immiscible fluids has been achieved in time-dependent creeping flows in two simple two-dimensional geometries. The first is the journal bearing arrangement, where two eccentric cylinders counter rotate alternately for a fixed time period. The second geometry is a cavity flow where the upper and lower walls are forced to move alternately, each parallel to itself but in opposite directions, using two independently driven timing belts. In both cases, good mixing is achieved after just few periods for certain optimum movement protocols.

Again for the creeping flow between two counter-rotating eccentric cylinders, Ghosh et al.[84] have computed the enhancement in the cross-stream heat (or mass) transport associated with either a steady recirculation region or chaotic advection. As compared to pure conduction (or molecular diffusion), the steady-state enhancement is proportional to the square root of a characteristic width of

the recirculation region, but the effect diminishes as the Péclet number is lowered from its asymptotic infinite value. If time-periodic forcing is used to perturb the steady recirculation region, 100% time-averaged enhancement over pure diffusion is achieved at the optimum forcing frequency leading to homoclinic entanglement of the recirculation region's bounding separatrices and, hence, to chaotic advection transport across those separatrices.

To avoid the practical difficulties of using time-periodic perturbations at a boundary, Acharya et al.[85] investigated analytically, numerically and experimentally the possibility of effecting chaotic advection in helical pipes by spatial periodicity in the downstream direction. Using as a base flow a conventional, fixed-axis coiled tube, they perturbed the customary secondary flow by periodic changes in the coiling. One such perturbation is shown in Fig. 9, where each successive loop of the coil lies on a different, mutually perpendicular plane. Chaotic particle paths are observed when the switching length exceeds the critical value of one-half of the loop circumference. As compared to a conventional coiled tube using realistic fluids (that is, finite Reynolds number, Prandtl number and Péclet number), the alternating-axis coiled heat exchanger leading to chaotic advection enhances the heat transfer by 6–8% with only a 1.5–2.5% pressure drop penalty. Heat transfer enhancement by chaotic advection is reviewed by Chang and Sen.[86]

The same alternating-axis coiled tube just described was investigated in an analytical study directed toward enhancing the rate of mass transfer. Sawyers et al.[87] documented the benefits of chaotic advection on the overall yield in a slow, bimolecular chemical reaction. The two reactants are initially separated and the flow is assumed laminar and steady with high mass Péclet number. In a straight tube, there is no flow in the transverse direction, and the interface separating the two reactants does not change as the flow progresses downstream. Mixing in this case is achieved solely by the very slow molecular diffusion process. Regular mixing produced by the secondary transverse flow in a helical coil linearly stretches the interface separating two reactants, which leads to some improvement in mixing. Chaotic mixing, by contrast, leads to an exponentially growing interface length that can be related to a positive Lyapunov exponent. The area-averaged product mass fraction increases proportionally in this case, which leads to a much higher yield of the reaction. Numerical solutions show that the enhancement by chaotic mixing also exists for fast reactions.

In a different kind of three-dimensional geometry, Sawyers et al.[88] computationally investigated the heat transfer enhancement in the laminar flow inside corrugated channels. They compared the regular mixing in two-dimensional sinusoidal corrugations (with primary flow perpendicular to the corrugations) to the chaotic mixing resulting when the corrugations are sinusoidal in two orthogonal directions. The conventional geometry and the egg-carton one are shown schematically in Fig. 10. As compared to flat-plate heat exchangers, the convection heat transfer coefficient is higher for the two-dimensional corrugations due to the presence of recirculation zones. The three-dimensional corrugations cause the boundary of those zones to be broken, thus allowing fluid particles to cross between the recirculation regions and the main flow. This allows heat transfer across what was a barrier to advection in the two-dimensional corrugated channel. The resulting enhanced mixing reduces the fluid temperature nonuniformities, thereby steepening the temperature gradient near the boundaries and increasing the heat transfer between the fluid and the channel walls.

In here, we ponder the possibility of introducing minute geometrical modifications to the lifting surfaces of MAV. The purpose of the microscopic grooves would be to effect chaotic mixing in the

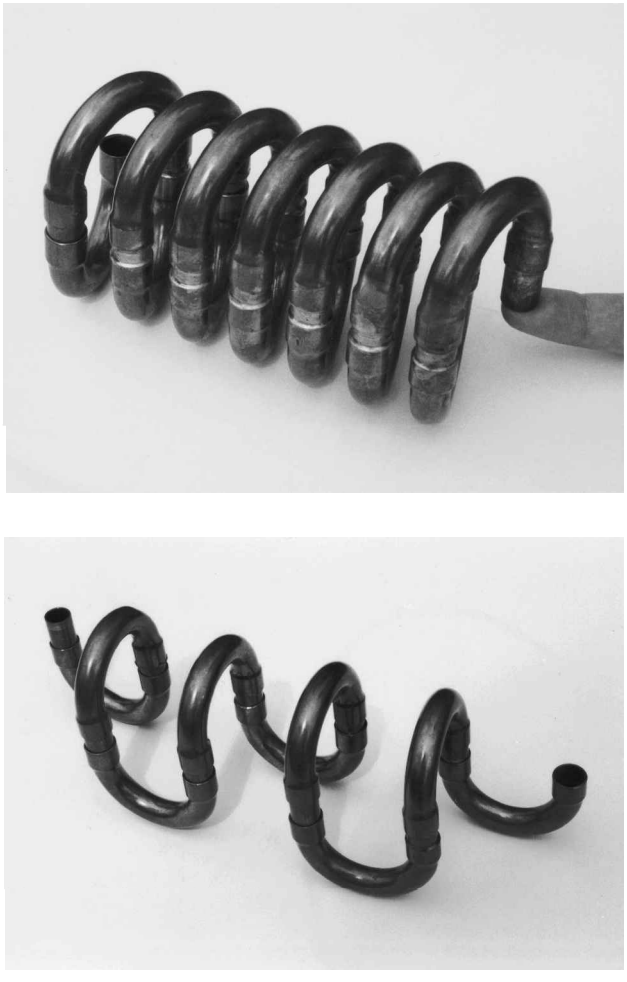

Fig. 9 Conventional coiled tube and alternating-axis tube.

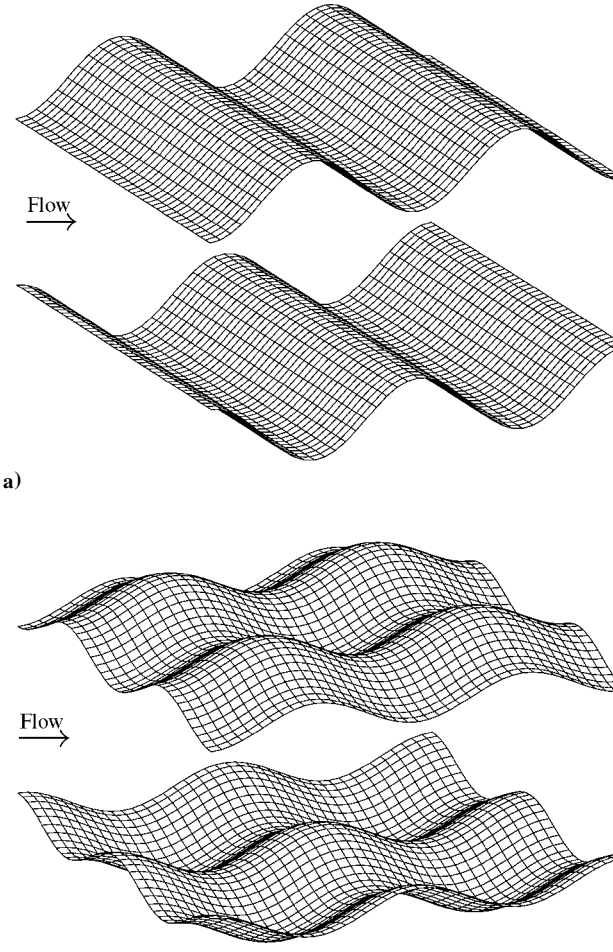


Fig. 10 Channels with a) two-dimensional corrugations and b) egg-carton corrugations.

near-wall laminar flow, thus delaying or preventing boundary-layer separation. The imposed roughness should be sufficiently small as to maintain a hydrodynamically smooth surface and, thus, to prevent the skin-friction drag from rising.

Finally, for readers desiring either a gentle primer or more detailed treatment, see Refs. 81 and 89–95 for a broad range of sophistication and readability on the topics of nonlinear dynamical systems theory, chaos and chaotic advection.

## V. Genetic Algorithms

We outline in this section the soft computing tool termed genetic algorithms. The idea here is to use such algorithm to optimize the shape of the lifting surface of a MAV to achieve maximum lift-to-drag ratio. The principal constituents of soft computing are neurocomputing, fuzzy logic, and genetic algorithms. These elements, together with probabilistic reasoning, can be combined in hybrid arrangements resulting in better systems in terms of parallelism, fault tolerance, adaptivity and uncertainty management.

Genetic algorithms are search algorithms based loosely on the mechanics of natural selection and natural genetics. They combine survival of the fittest among string structures with structured yet randomized information exchange and are used for search, optimization and machine learning. For control, genetic algorithms aim at achieving minimum cost function and maximum performance measure while satisfying the problem constraints. Goldberg,[96] Davis,[97] and Holland[98] provide introduction to the field.

In the Darwinian principle of natural selection, the fittest members of a species are favored to produce offspring. Even biologists cannot help but being awed by the complexity of life observed to evolve in the relatively short time suggested by the fossil records. A living being is an amalgam of characteristics determined by the (typically tens of thousands) genes in its chromosomes. Each gene may have several forms or alternatives called alleles, which produce differences in the set of characteristics associated with that gene. The chromosomes are, therefore, the organic devices through which the structure of a creature is encoded, and this living being is created partly through the process of decoding those chromosomes. Genes transmits hereditary characters and form specific parts of a self-perpetuated deoxyribonucleic acid in a cell nucleus. Natural selection is the link between the chromosomes and the performance of their decoded structures. Simply put, the process of natural selection causes those chromosomes that encode successful structures to reproduce more often than those that do not.

In an attempt to solve difficult problems, John H. Holland of the University of Michigan introduced in the early 1970s the fabricated version of the procedure of natural evolution. The candidate solutions to a problem are ranked by the genetic algorithm according to how well they satisfy a certain criterion, and the fittest members are the most favored to combine amongst themselves to form the next generation of the members of the species. Fitter members presumably produce even fitter offspring and, therefore, better solutions to the problem at hand. Solutions are represented by binary strings; each trial solution is coded as a vector called chromosome. The elements of a chromosome are described as genes, and its varying values at specific positions are called alleles. Good solutions are selected for reproduction based on a fitness function using genetic recombination operators such as crossover and mutation. The main advantage of genetic algorithms is their global parallelism in which the search efforts to many regions of the search area are simultaneously allocated.

Genetic algorithms (GA) have been used for shape optimization, as for example, the optimization of a duct shape to maximize the flow from a viscous pump.[99] GA has also been used in conjunction with an Euler code to optimize the shape of a very high Reynolds number airfoil.[100] However, to the author's knowledge and at the time of writing this paper, the optimization of the airfoil section of an MAV using a Navier–Stokes code is yet to benefit from this powerful soft computing tool. Clearly, the low Reynolds numbers involved in MAV necessitate the use of a viscous, in contrast to a potential, code.

## VI. Concluding Remarks

In this paper we pondered whether MEMS can help improving the performance of MAV. The paper focused on the lifting and control surfaces of MAV particularly the fixed-wing type. At the extremely low Reynolds numbers associated with MAV, microsensors and microactuators can be used instead of traditional flow control strategies to delay or prevent separation. MEMS can also be used instead of bulky control surfaces such as the traditional mechanical flaps acting as ailerons, elevators, and rudders. The paper additionally discussed the possibility of employing chaotic mixing to delay laminar separation and using genetic algorithms in conjunction with a Navier–Stokes code to search for the optimum profile of the lifting surface of an MAV.

## References


[1]Canan, J. W., "Seeing More, and Risking Less, with UAVs," *Aeropsace America*, Vol. 37, No. 10, 1999, pp. 26–35.

[2]Dornheim, M. A., "Several Micro Air Vehicles in Flight Test Programs," *Aviation Week and Space Technology*, Vol. 151, No. 2, 12 July 1999, pp. 47, 48.

[3]Carmichael, B. H., "Low Reynolds Number Airfoil Survey," NASA CR-165803, 1981.

[4]McMasters, J. H., and Henderson, M. L., "Low Speed Single Element Airfoil Synthesis," *Technical Soaring*, Vol. 6, 1980, pp. 1–21.

[5]Lerner, E. J., "Insect Flight Elucidated," *Industrial Physicist*, Vol. 5, No. 5, 1999, pp. 6–8.

[6]McCullough, G. B., and Gault, D. E., "Examples of Three Representative Types of Airfoil-Section Stall at Low Speed," NACA TN 2502, 1951.

[7]Lissaman, P. B. S., "Low-Reynolds-Number Airfoils," *Annual Review of Fluid Mechanics*, Vol. 15, 1983, pp. 223–239.

[8]Tani, I., "Low-Speed Flows Involving Bubble Separations," *Progress in Aeronautical Science*, Vol. 5, edited by D. Küchemann and L. H. G. Sterne, Pergamon, New York, 1964, pp. 70–103.

[9]Gad-el-Hak, M., "Flow Control: The Future," *Journal of Aircraft*, Vol. 38, No. 3, 2001, pp. 402–418.

[10]Mueller, T. J. (1985a), "Low Reynolds Number Vehicles," AGARDograph 288, AGARD, NATO, Neuilly-sur-Seine, France, 1985.

[11]Gad-el-Hak, M., "Control of Low-Speed Airfoil Aerodynamics," *AIAA Journal*, Vol. 28, 1990, pp. 1537–1552.

[12]Mueller, T. J. (ed.), *Proceedings of the Conference on Low Reynolds Number Airfoil Aerodynamics*, Univ. of Notre Dame, Notre Dame, IN, 1985.

[13]Mueller, T. J. (ed.), *Proceedings of the Conference on Low Reynolds Number Aerodynamics*, Univ. of Notre Dame, Notre Dame, IN, 1989.

[14]Mueller, T. J. (ed.), *Proceedings of the Conference on Fixed, Flapping and Rotary Wing Vehicles at Very Low Reynolds Numbers*, Univ. of Notre Dame, Notre Dame, IN, 2000.

[15]Von Doenhoff, A. E., "A Method of Rapidly Estimating the Position of the Laminar Separation Point," NACA TN 671, 1938.

[16]Thwaites, B., "Approximate Calculations of the Laminar Boundary Layer," *Aeronautical Quarterly*, Vol. 1, 1949, pp. 245–280.

[17]Torres, G. E., and Mueller, T. J., "Aerodynamic Characteristics of Low-Aspect-Ratio Wings at Low Chord-Reynolds-Numbers," *Proceedings of the Conference on Fixed, Flapping and Rotary Wing Vehicles at Very Low Reynolds Numbers*, edited by T. J. Mueller, Univ. of Notre Dame, Notre Dame, IN, 2000.

[18]Jones, B. M., "Stalling," *Journal of the Royal Aeronautical Society*, Vol. 38, 1934, pp. 753–770.

[19]Schmitz, F. W., "Aerodynamics of the Model Airplane, Part I, Airfoil Measurements," NASA-TM-X-60976, 1967.

[20]Mueller, T. J., "The Influence of Laminar Separation and Transition on Low Reynolds Number Airfoil Hysteresis," *Journal of Aircraft*, Vol. 22, 1985, pp. 763–770.

[21]Bastedo, W. G., Jr., and Mueller, T. J., "Performance of Finite Wings at Low Reynolds Numbers," *Proceedings of the Conference on Low Reynolds Number Airfoil Aerodynamics*, edited by T. J. Mueller, Univ. of Notre Dame, Notre Dame, IN, 1985, pp. 195–205.

[22]Brendel, M., and Mueller, T. J., "Boundary Layer Measurements on an Airfoil at a Low Reynolds Number in an Oscillating Freestream," *AIAA Journal*, Vol. 26, 1988, pp. 257–263.

[23]Crabtree, L. F., "Effects of Leading-Edge Separation on Thin Wings in Two-Dimensional Incompressible Flow," *Journal of the Aeronautical Sciences*, Vol. 24, 1957, pp. 597–604.

[24]Burns, T. F., "Experimental Studies of Eppler 61 and Pfenninger 048 Airfoils at Low Reynolds Numbers," M.Sc. Thesis, Univ. of Notre Dame, Notre Dame, IN, 1981.

[25]Mueller, T. J., and Burns, T. F., "Experimental Studies of the Eppler 61 Airfoil at Low Reynolds Numbers," AIAA Paper 82-0345, Tokyo, Japan, June 1982.

[26]Render, P. M., "The Experimental and Theoretical Aerodynamics of Aerofoil Sections Suitable for Remotely Piloted Vehicles," Ph.D. Dessertation, Cranfield Inst. of Technology, Cranfield, England, U.K., 1984.

[27]Render, P. M., Stollery, J. L., and Williams, B. R., "Aerofoils at Low Reynolds Numbers—Prediction and Experiments," *Numerical and Physical Aspects of Aerodynamic Flows III*, edited by T. Cebeci, Springer-Verlag, New York, 1985, pp. 155–167.

[28]Liebeck, R. H., and Camacho, P. P., "Airfoil Design at Low Reynolds Number with Constrained Pitching Moment," *Proceeding of the Conference on Low Reynolds Number Airfoil Aerodynamics*, edited by T. J. Mueller, Univ. of Notre Dame, Notre Dame, IN, 1985, pp. 27–51.

[29]Bastedo, W. G., Jr., and Mueller, T. J., "Spanwise Variation of Laminar Separation Bubbles on Wings at Low Reynolds Numbers," *Journal of Aircraft*, Vol. 23, 1986, pp. 687–694.

[30]Stollery, J. L., and Dyer, D. J., "Wing-Section Effects on the Flight Performance of a Remotely Piloted Vehicle," *Journal of Aircraft*, Vol. 26, 1989, pp. 932–938.

[31]Crabtree, L. F., "The Formation of Regions of Separated Flow on Wing Surfaces. Part I: Low-Speed Tests on a Two-Dimensional Unswept Wing with a 10% Thick RAE—101 Section," Royal Aerospace Establishment, Rept. Aero. 2528, Farnborough, England, U.K., 1954.

[32]Fitzgerald, E. J., and Mueller, T. J., "Measurements in a Separation Bubble on an Airfoil Using Laser Velocimetry," *AIAA Journal*, Vol. 28, 1990, pp. 584–592.

[33]McCullough, G. B., "The Effect of Reynolds Number on the Stalling Characteristics and Pressure Distributions of Four Moderately Thin Airfoil Sections," NACA TN-3524, 1955.

[34]Angell, J. B., Terry, S. C., and Barth, P. W., "Silicon Micromechanical Devices," *Faraday Transactions I*, Vol. 68, 1983, pp. 744–748.

[35]Gabriel, K. J., Jarvis, J., and Trimmer, W. (eds.), *Small Machines, Large Opportunities: A Report on the Emerging Field of Microdynamics*, AT&T Bell Labs., Murray Hill, NJ, 1988.

[36]Gabriel, K. J., Tabata, O., Shimaoka, K., Sugiyama, S., and Fujita, H., "Surface-Normal Electrostatic/Pneumatic Actuator," *Proceedings of the IEEE Micro Electro Mechanical Systems '92*, Inst. of Electrical and Electronics Engineers, New York, 1992, pp. 128–131.

[37]O'Connor, L., "MEMS: Micromechanical Systems," *Mechanical Engineering*, Vol. 114, Feb. 1992, pp. 40–47.

[38]Gravesen, P., Branebjerg, J., and Jensen, O. S., "Microfluidics—A Review," *Journal of Micromechanics Microengineering*, Vol. 3, 1993, pp. 168–182.

[39]Bryzek, J., Peterson, K., and McCulley, W., "Micromachines on the March," *IEEE Spectrum*, Vol. 31, May 1994, pp. 20–31.

[40]Gabriel, K. J., "Engineering Microscopic Machines," *Scientific American*, Vol. 260, Sept. 1995, pp. 150–153.

[41]Hogan, H., "Invasion of the Micromachines," *New Scientist*, Vol. 29, June 1996, pp. 28–33.

[42]Ho, C.-M., and Tai, Y.-C., "Review: MEMS and Its Applications for Flow Control," *Journal of Fluids Engineering*, Vol. 118, 1996, pp. 437–447.

[43]Ho, C.-M., and Tai, Y.-C., "Micro-Electro-Mechanical Systems (MEMS) and Fluid Flows," *Annual Review of Fluid Mechanics*, Vol. 30, 1998, pp. 579–612.

[44]Tien, N. C., "Silicon Micromachined Thermal Sensors and Actuators," *Microscale Thermophysical Engineering*, Vol. 1, 1997, pp. 275–292.

[45]Busch-Vishniac, I. J., "Trends in Electromechanical Transduction," *Physics Today*, Vol. 51, July 1998, pp. 28–34.

[46]Amato, I., "Formenting a Revolution, in Miniature," *Science*, Vol. 282, No. 5388, 16 Oct. 1998, pp. 402–405.

[47]Paula, G., "MEMS Sensors Branch Out," *Aerospace America*, Vol. 34, Sept. 1996, pp. 26–32.

[48]Ouellette, J., "MEMS: Mega Promise for Micro Devices," *Mechanical Engineering*, Vol. 118, Oct. 1996, pp. 64–68.

[49]Ashley, S., "Getting a Microgrip in the Operating Room," *Mechanical Engineering*, Vol. 118, Sept. 1996, pp. 91–93.

[50]Robinson, E. Y., Helvajian, H., and Jansen, S. W., "Small and Smaller: The World of MNT," *Aerospace America*, Vol. 34, Sept. 1996, pp. 26–32.

[51]Robinson, E. Y., Helvajian, H., and Jansen, S. W., "Big Benefits from Tiny Technologies," *Aerospace America*, Vol. 34, Oct. 1996, pp. 38–43.

[52]Lipkin, R., "Micro Steam Engine Makes Forceful Debut," *Science News*, Vol. 144, Sept. 1993, p. 197.

[53]Bandyopadhyay, P. R., Breuer, K. S., and Blechinger, C. J. (ed.), *Application of Microfabrication to Fluid Mechanics*, FED Vol. 197, American Society of Mechanical Engineers, New York, 1994.

[54]Breuer, K. S., Bandyopadhyay, P. R., and Gad-el-Hak, M. (eds.), *Application of Silicon Microfabrication to Fluid Mechanics*, DSC Vol. 59, American Society of Mechanical Engineers, New York, 1996.

[55]Gad-el-Hak, M., "Interactive Control of Turbulent Boundary Layers: A Futuristic Overview," *AIAA Journal*, Vol. 32, 1994, pp. 1753–1765.

[56]Gad-el-Hak, M., "Modern Developments in Flow Control," *Applied Mechanics Reviews*, Vol. 49, 1996, pp. 365–379.

[57]Gad-el-Hak, M., *Flow Control: Passive, Active and Recative Flow Management*, Cambridge Univ. Press, London, 2000.

[58]Lumley, J. L., "Control of Turbulence," AIAA Paper 96-0001, 1996.

[59]McMichael, J. M., "Progress and Prospects for Active Flow Control Using Microfabricated Electromechanical Systems (MEMS)," AIAA Paper 96-0306, 1996.

[60]Mehregany, M., DeAnna, R. G., and Reshotko, E., "Microelectromechanical Systems for Aerodynamics Applications," AIAA Paper 96-0421, 1996.

[61]Löfdahl, L., Glavmo, M., Johansson, B., and Stemme, G., "A Silicon Transducer for the Determination of Wall-Pressure Fluctuations in Turbulent Boundary Layers," *Applied Scientific Research*, Vol. 51, 1993, pp. 203–207.

[62]Löfdahl, L., Kälvesten, E., and Stemme, G., "Small Silicon Based Pressure Transducers for Measurements in Turbulent Boundary Layers," *Experiments in Fluids*, Vol. 17, 1994, pp. 24–31.

[63]Löfdahl, L., and Gad-el-Hak, M., "MEMS Applications in Turbulence and Flow Control," *Progress in Aerospace Sciences*, Vol. 35, 1999, pp. 101–203.

[64]Löfdahl, L., and Gad-el-Hak, M., "MEMS-Based Pressure and Shear Stress Sensors," *Measurement Science and Technology*, Vol. 10, 1999, pp. 665–686.

[65]Warkentin, D. J., Haritonidis, J. H., Mehregany, M., and Senturia, S. D., "A Micromachined Microphone with Optical Interference Readout," *Proceedings of the Fourth International Conference on Solid-State Sensors and Actuators (Transducers '87)*, 1987.

[66]Young, A. M., Goldsberry, J. E., Haritonidis, J. H., Smith, R. I., and Senturia, S. D., "A Twin-Interferometer Fiber-Optic Readout for Diaphragm Pressure Transducers," *IEEE Solid-State Sensor and Actuator Workshop*, Inst. of Electrical and Electronics Engineers, New York, 1988.

[67]Haritonidis, J. H., Senturia, S. D., Warkentin, D. J., and Mehregany, M., "Optical Micropressure Transducer," U.S. Patent 4,926,696, 1990.

[68]Haritonidis, J. H., Senturia, S. D., Warkentin, D. J., and Mehregany, M., "Pressure Transducer Apparatus," U.S. Patent, 4,942,767, 1990.

[69]Halsey, T. C., and Martin, J. E., "Electrorheological Fluids," *Scientific American*, Vol. 269, Oct. 1993, pp. 58–64.

[70]Wiltse, J. M., and Glezer, A., "Manipulation of Free Shear Flows Using Piezoelectric Actuators," *Journal of Fluid Mechanics*, Vol. 249, 1993, pp. 261–285.

[71]James, R. D., Jacobs, J. W., and Glezer, A., "Experimental Investigation of a Turbulent Jet Produced by an Oscillating Surface Actuator," *Applied Mechanics Reviews*, Vol. 47, No. 6, Pt. 2, 1994, pp. S127–S1131.

[72]Jacobson, S. A., and Reynolds, W. C., "An Experimental Investigation Towards the Active Control of Turbulent Boundary Layers," Dept. of Mechanical Engineering, Rept. TF-64, Stanford Univ., Stanford, CA, 1995.

[73]Vargo, S. E., and Muntz, E. P., "A Simple Micromechanical Compressor and Vacuum Pump for Flow Control and Other Distributed Applications," AIAA Paper 96-0310, 1996.

[74]Keefe, L. R., "A MEMS-Based Normal Vorticity Actuator for Near-Wall Modification of Turbulent Shear Flows," *Proceedings of the Workshop on Flow Control: Fundamentals and Practices*, edited by J.-P. Bonnet, M. Gad-el-Hak, and A. Pollard, Institut d'Etudes Scientifique des Cargèse, Corsica, France, 1–5 July 1996, pp. 1–21.

[75]Sen, M., Wajerski, D., and Gad-el-Hak, M., "A Novel Pump for MEMS Applications," *Journal of Fluids Engineering*, Vol. 118, 1996, pp. 624–627.

[76]Sharatchandra, M. C., Sen, M., and Gad-el-Hak, M., "Navier–Stokes Simulations of a Novel Micropump," *Symposium on Application of Microfabrication to Fluid Mechanics*, DSC-Vol. 59, edited by K. S. Breuer, P. R. Bandyopadhyay, and M. Gad-el-Hak, American Society of Mechanical Engineers, New York, 1996, pp. 225–238.

[77]Sharatchandra, M. C., Sen, M., and Gad-el-Hak, M., "Navier–Stokes Simulations of a Novel Viscous Pump," *Journal of Fluids Engineering*, Vol. 119, 1997, pp. 372–382.

[78]Liepmann, H. W., and Nosenchuck, D. M., "Active Control of Laminar-Turbulent Transition," *Journal of Fluid Mechanics*, Vol. 118, 1982, pp. 201–204.

[79]Liepmann, H. W., Brown, G. L., and Nosenchuck, D. M., "Control of Laminar Instability Waves Using a New Technique," *Journal of Fluid Mechanics*, Vol. 118, 1982, pp. 187–200.

[80]Aref, H., "Stirring by Chaotic Advection," *Journal of Fluid Mechanics*, Vol. 143, 1984, pp. 1–21.

[81]Ottino, J. M., *The Kinematics of Mixing: Stretching, Chaos, and Transport*, Cambridge Univ. Press, Cambridge, England, U.K., 1989.

[82]Ottino, J. M., "The Mixing of Fluids," *Scientfic American*, Vol. 260, Jan. 1989, pp. 56–67.

[83]Ottino, J. M., "Mixing, Chaotic Advection, and Turbulence," *Annual Review of Fluid Mechanics*, Vol. 22, 1990, pp. 207–253.

[84]Ghosh, S., Chang, H.-C., and Sen, M., "Heat-Transfer Enhancement due to Slender Recirculation and Chaotic Transport Between Counter-Rotating Eccentric Cylinders," *Journal of Fluid Mechanics*, Vol. 238, 1992, pp. 119–154.

[85]Acharya, N., Sen, M., and Chang, H.-C., "Heat Transfer Enhancement in Coiled Tubes by Chaotic Mixing," *International Journal of Heat and Mass Transfer*, Vol. 35, 1992, pp. 2475–2489.

[86]Chang, H.-C., and Sen, M., "Application of Chaotic Advection to Heat Transfer," *Chaos Applied to Fluid Mixing*, edited by H. Aref and M. S. El Naschie, Pergamon Press, Oxford, England, U.K., 1995, pp. 211–231.

[87]Sawyers, D. R., Sen, M., and Chang, H.-C., "Effect of Chaotic Interfacial Stretching on Bimolecular Chemical Reaction in Helical-Coil Reactors," *Chemical Engineering Journal*, Vol. 64, 1996, pp. 129–139.

[88]Sawyers, D. R., Sen, M., and Chang, H.-C., "Heat Transfer Enhancement in Three-Dimensional Corrugated Channel Flow," *International Journal of Heat and Mass Transfer*, Vol. 41, 1998, pp. 3559–3573.

[89]Gleick, J., *Chaos—Making a New Science*, Viking, New York, 1987.

[90]Baker, G. L., and Gollub, J. P., *Chaotic Dynamics—an Introduction*, Cambridge Univ. Press, Cambridge, England, U.K., 1990.

[91]Kim, J. H., and Stringer, J. (eds.), *Applied Chaos*, Wiley, New York, 1992.

[92]Moon, F. C., *Chaotic and Fractal Dynamics—An Introduction for Applied Scientists and Engineers*, Wiley, New York, 1992.

[93]Ott, E., *Chaos in Dynamical Systems*, Cambridge Univ. Press, Cambridge, England, U.K., 1993.

[94]Aref, H., and El Naschie, M. S. (eds.), *Chaos Applied to Fluid Mixing*, Pergamon Press, Oxford, England, U.K., 1995.

[95]Nayfeh, A. H., and Balachandran, B., *Applied Nonlinear Dynamics—Analytical, Computational, and Experimental Methods*, Wiley, New York, 1995.

[96]Goldberg, D. E., *Genetic Algorithms in Search, Optimization, and Machine Learning*, Addison Wesley Longman, Reading, MA, 1989.

[97]Davis, L. (ed.), *Handbook of Genetic Algorithms*, Van Nostrand Reinhold, New York, 1991.

[98]Holland, J. H., *Adaptation in Natural and Artificial Systems*, MIT Press, Cambridge, MA, 1992.

[99]Sharatchandra, M. C., Sen, M., and Gad-el-Hak, M., "A New Approach to Constrained Shape Optimization Using Genetic Algorithms," *AIAA Journal*, Vol. 36, 1998, pp. 51–61.

[100]Fanjoy, D. W., and Crossley, W. A., "Aerodynamic Shape Design for Rotor Airfoils via Genetic Algorithm," *Journal of the American Helicopter Society*, Vol. 43, No. 3, 1998, pp. 263–270.